

Scalelengths in Dark Matter Halos

Eric I. Barnes, Liliya L. R. Williams

Department of Astronomy, University of Minnesota, Minneapolis, MN 55455

barnes@astro.umn.edu

llrw@astro.umn.edu

Arif Babul¹

Department of Physics and Astronomy, University of Victoria, BC, Canada

babul@uvic.ca

Julianne J. Dalcanton²

Astronomy Department, University of Washington, Box 351580, Seattle, WA 98195

jd@astro.washington.edu

ABSTRACT

We investigate a hypothesis regarding the origin of the scalelength in halos formed in cosmological N-body simulations. This hypothesis can be viewed as an extension of an earlier idea put forth by Merritt and Aguilar. Our findings suggest that a phenomenon related to the radial orbit instability is present in such halos and is responsible for density profile shapes. This instability sets a scalelength at which the velocity dispersion distribution changes rapidly from isotropic to radially anisotropic. This scalelength is reflected in the density distribution as the radius at which the density profile changes slope. We have tested the idea that radially dependent velocity dispersion anisotropy leads to a break in density profile shape by manipulating the input of a semi-analytic model to imitate the velocity structure imposed by the radial orbit instability. Without such manipulation, halos formed are approximated by single power-law density profiles and isotropic velocity distributions. Halos formed with altered inputs display density distributions featuring scalelengths and anisotropy profiles similar to those seen in cosmological N-body simulations.

Subject headings: dark matter—galaxies:formation, evolution

1. Introduction

Some of the earliest studies to lay the foundation of galaxy formation have relied on analytical methods to follow the collisionless evolution of dark matter (*e.g.*, Gunn & Gott 1972; Gott 1975; Gunn 1977) and lead to pure power-law density distributions. Several other studies

have built on this early analytical framework. Fillmore & Goldreich (1983) and Bertschinger (1984) have found similarity solutions for the spherical collapse of cosmological perturbations that produce nearly pure power-law density profiles. The halos in these studies are populated solely by radial orbits. Ryden & Gunn (1987) have introduced nonradial motion, but the resulting density profiles are still well-approximated by a single power-law over at least two orders of magnitude in radius, with noticeable deviations only on small

¹Leverhulme Visiting Professor, Universities of Oxford and Durham

²Alfred P. Sloan Foundation Fellow

$[\log(r/r_{\text{vir}}) \lesssim -2]$ and large $[\log(r/r_{\text{vir}}) \gtrsim 0]$ scales (r_{vir} is the virial radius).

As computing power has increased, another approach has been adopted to investigate cosmological structure formation, N-body simulations. These studies do not suffer from the same limitations of adopted approximations that are inherent in the analytically-based work, however such simulations do rely on other approximations, like gravitational softening. Given appropriate initial conditions, cosmological N-body simulations (CNS) can follow structure formation through non-linear development and investigate the impact of hierarchical merging (*e.g.*, Dubinski & Carlberg 1991; Navarro *et al.* 1996, 1997; Moore *et al.* 1998, 1999; Bullock *et al.* 2001; Power *et al.* 2003). These studies agree that the equilibrium dark matter halos that form in CNS have nearly universal density profiles that are nothing like single power-laws. These halos generically have logarithmic slopes $\gamma = -d \log \rho / d \log r$ that become larger with increasing radius; $\gamma \approx 1$ at one-hundredth of a virial radius and $\gamma \approx 3$ near the virial radius. There remain, however, disagreements regarding the exact values and behavior of γ , especially at small radii.

The fitting function that has been widely used to characterize the density profiles of CNS halos, the NFW profile (Navarro *et al.* 1996), has an explicit scalelength that divides the inner and outer behaviors. The NFW profile γ asymptotes to 1 as $r \rightarrow 0$ and 3 as $r \rightarrow \infty$. Recently, Navarro *et al.* (2004) have discussed another fitting function to describe the density profiles of higher resolution CNS halos. Unlike the NFW profile, γ of the new function does not approach asymptotic values at small and large radii and does not have the same well-defined scalelength as the NFW profile. Instead, γ of this new profile changes continuously with radius, implying that there are no regions in which the density profile behaves like a power-law. At the same time, another recent study (Diekmann *et al.* 2005) finds that the $r \rightarrow 0$ asymptotic power-law behavior persists in their high resolution CNS. Given this disagreement, it is unclear whether or not CNS halos actually have preferred scalelengths. However, the NFW profile does provide a reasonable description of density distributions for galaxy and cluster scale CNS halos (Merritt *et al.* 2005). For the sake of brevity, we will refer to the radius at which $\gamma = 2$ as the scale-

length.

Despite these fairly minor disagreements regarding the behavior of γ , CNS halos (as a class) appear qualitatively similar. This similarity does not extend to the analytically-based (AB) halos described above. Like previous studies that have sought to understand the differences between CNS and AB halos (*e.g.*, Avila-Reese, Firmani, & Hernandez 1998; Lokas 2000; Nusser 2001), we are investigating how the input physics differs between the methods and whether or not such physics can explain the differences. We find evidence that a phenomenon related to the radial orbit instability (ROI) can account for the differences as well as shed some light on the universality and scalelengths of CNS halos.

A brief introduction to the ROI is given in §2. We lay out the hypothesis, drawing links between the ROI, CNS halos, and AB halos, in §3. The demonstration of the hypothesis relies on evolving dark matter halos semi-analytically and is based on the method presented in Ryden & Gunn (1987). Our modifications to this method have been fully discussed in Williams *et al.* (2004). Briefly, this method relies on spherical symmetry and ignores complications due to merging. This simplicity provides us with a degree of control not present in CNS. At the same time, inclusion of secondary perturbations allows us to approximate the correct evolution of an isolated dark matter halo. Details of the method and results of testing the hypothesis are presented in §4. We discuss the link between the ROI and the shapes of CNS halo density profiles in §5. The final section summarizes and presents the conclusions drawn from this work.

2. Overview of the Radial Orbit Instability

Early analytical and N-body studies have found that equilibrium spherical systems composed of purely radial orbits are unstable to forming bars or triaxial systems (Polyachenko 1981; Fridman & Polyachenko 1984; Binney & Tremaine 1987, §5.2). Although there is no general theory explaining the ROI, Palmer & Papaloizou (1987) argue that if a spherical system develops a small $m = 2$ distortion, precession of radial orbits can draw them to reinforce the distortion, thereby increasing the distortion and leading to bar formation. Whatever

the exact mechanism is, it is clear that nonradial forces play a key role, as we will discuss in the next section.

Merritt & Aguilar (1985) have further investigated the ROI by creating equilibrium systems with initial anisotropy ($\beta = 1 - \sigma_\phi^2/\sigma_r^2$) profiles described by,

$$\beta(r) = \frac{r^2}{r_a^2 + r^2}, \quad (1)$$

where r_a is referred to as the anisotropy radius (Merritt 1985). These profiles are completely isotropic ($\beta = 0$) for $r_a/r_{1/2} = \infty$, where $r_{1/2}$ is the initial half-mass radius. For smaller $r_a/r_{1/2}$ values, the anisotropy increases from the center outwards. At the limit $r_a/r_{1/2} = 0$, the entire model is composed of radial orbits. Merritt & Aguilar (1985) list several fundamental results of the ROI. First, an initially spherical system that undergoes the ROI transforms into a nearly prolate bar with long-to-short axis ratio $\approx 2 - 2.5$. Second, for the anisotropy profile of Equation 1 there appears to be a fairly distinct border between systems that form a significant bar ($r_a/r_{1/2} \lesssim 0.2$) and those that remain relatively spherical ($r_a/r_{1/2} \gtrsim 0.3$); however, other anisotropy profiles produce different stability criteria. Third, the global anisotropy measure $2T_r/T_t$ (where T_r and T_t are the kinetic energies associated with radial and tangential motions, respectively) is not a universal arbiter of whether or not a system is unstable; larger values of this ratio indicate instability, but there does not appear to be a definitive demarcation value (Polyachenko & Shukhman 1981; Barnes, Goodman, & Hut 1986). The Merritt & Aguilar (1985) work also highlights that the stability of any equilibrium system depends (at a minimum) on the anisotropy distribution, with centrally isotropic systems being more stable than those with radially anisotropic cores. In brief, collisionless systems will undergo the ROI if a sufficient fraction of orbits are predominantly radial.

While we have so far discussed the ROI in equilibrium systems, collisionless collapses also appear to relate to the ROI. The link with the ROI is that these cold collapses produce mostly radial motion, a condition favorable to the onset of the ROI. We compare the results of noncosmological and cosmological collapses and discuss the signature of

the ROI in the next section.

3. Collapses & the Radial Orbit Instability

Studies of cold collisionless collapses in non-cosmological settings (van Albada 1982; McGlynn 1984; Aguilar & Merritt 1990; Trenti, Bertin, & van Albada 2005) report that the end results of collapses are good descriptions of observed surface brightness profiles of elliptical galaxies. For example, the collapses presented in van Albada (1982) result in mildly nonspherical systems with two-dimensional projected density profiles that are well-approximated by the Sérsic function $\ln(\Sigma/\Sigma_e) = -b_n[(R/R_e)^{1/n} - 1]$ (Sérsic 1968), with $n \approx 4$ like a de Vaucouleurs profile. These collapse products also display characteristic anisotropy profiles; the inner regions are isotropic and transitions to radial anisotropy occur at larger radii. Merritt & Aguilar (1985) also point out that such collapses are less centrally concentrated than purely radial collapses. We extend and focus these thoughts by specifically investigating the link between density scalelengths and monotonic variations in velocity anisotropy.

While some choices of initial conditions in the previously mentioned studies have an eye towards describing cosmological situations, their main goals relate to understanding elliptical galaxies. Two studies directly deal with the differences between cosmological and noncosmological collapses. Katz (1991) argues that the ROI does not occur in cosmological settings because there is no correlation between final shape and initial $2T/W$ value. However, this study also reports that the final states of collapses have density profiles that are well-approximated by a Jaffe distribution (Jaffe 1983), which is similar to a de Vaucouleurs (Sérsic $n = 4$) profile when projected to two dimensions. More importantly, it is stated that the equilibria are supported by anisotropic velocity dispersions, like the results of the noncosmological studies. Carpintero & Muzzio (1995) find that realistic cosmological collapses do not succumb to the bar instability, but, like Katz (1991), the final density profiles are approximated by a Jaffe distribution (again, similar to an $n = 4$ Sérsic profile). Unfortunately, this study focuses solely on the final shapes of the collapses and does not present any kinematic information to allow a com-

parison of anisotropy profiles. Beyond these two studies, it is well-reported that halos formed in CNS tend to appear similar to the products of noncosmological collapse simulations; *i.e.*, they appear prolate spheroidal/triaxial (*e.g.*, Cole & Lacey 1996; Springel, White, & Hernquist 2004) and have monotonically increasing anisotropy distributions (Cole & Lacey 1996; Huss *et al.* 1999). All of these points lead us to conclude that cosmological collapse simulations result in systems that have the same qualitative density and anisotropy profiles as those from noncosmological studies.

The final states of these collapses are similar, but have the systems undergone the ROI? From the literature, it appears that most researchers consider bar formation to be the signpost of the instability. The Katz (1991) and Carpintero & Muzzio (1995) studies suggest that the ROI is absent in cosmological situations due to the lack of bars. Aguilar & Merritt (1990) refer to the merely slightly nonspherical results in van Albada (1982) as stable.

We propose that bar formation may not be the only sign of the ROI, but possibly only the most flagrant. The end results of collapses like those in van Albada (1982), where no strong bar is formed, display a less drastic result of the ROI. The equilibrium states resulting from collisionless collapses have similar anisotropy profiles; anisotropy increases (becomes more radial) with radius. This is in line with the discussion in Merritt & Aguilar (1985) which regards systems with isotropic central regions as more stable than those with radially anisotropic central regions. From this point of view, the ROI changes the mostly radial initial velocity distribution into one that has an isotropic core surrounded by a radial “mantle”. As we continue this discussion, we will use the term “mROI” (mild aspect of the ROI) to include the onset of the anisotropy profile and possible mild triaxiality and to distinguish it from the usual (and more extreme) bar-formation criterion.

Figure 1 shows anisotropy profiles that can be constructed from information in several previous studies. Panel a) shows the results of van Albada (1982) (plus symbols) and the analytical expression utilized by Merritt & Aguilar (1985), Equation 1. In the figure, we have set $r_a = r_e$, where r_e is the effective radius of the corresponding de Vaucouleurs profile. Note that the analytical ex-

pression is not a fit to the data points, it merely illustrates the initial anisotropy profile utilized in the ROI study of Merritt & Aguilar (1985). Panel b) shows the results from the “ $n = -2$ ” (here, n refers to the power spectrum $P(k) \propto k^n$, not the Sérsic profile) simulation of Cole & Lacey (1996) (asterisks) as well as the analytical expression adopted by Carlberg *et al.* (1997),

$$\beta = \beta_m \frac{4r/r_{178}}{4 + (r/r_{178})^2}, \quad (2)$$

where r_{178} is the virial radius and we have chosen $\beta_m = 0.3$. This expression is intended to fit the data points from equilibrium systems. The last panel shows the results of the simulations of Huss *et al.* (1999). Admittedly, the amplitude of the anisotropy in the Cole & Lacey (1996) result (panel b) is much smaller than the other cases, but the monotonically increasing nature is still present. The mROI anisotropy profile is found generically in collapses.

We find support for a link between the mROI and the presence of scalelengths in CNS halos looking closely at the information from Huss *et al.* (1999). This work has investigated 5 models of isolated dark matter halo formation. Four of these have simple initial conditions that were chosen to highlight the impact of differing amounts of initial random motion. The fifth represents a standard NFW type halo. Their Model I is especially interesting since it has no initial tangential motions and tangential forces are not allowed, essentially forcing radial collapse. The resulting halo is described by a constant radial anisotropy ($\beta = 1$, diamonds in Figure 1c) and a single power-law density profile $\rho \propto r^{-2}$. Once this restriction on tangential motion is lifted (Models II-IV have increasing amounts of initial random motion and allow nonradial forces), the resulting anisotropy profiles show basically isotropic cores with β increasing with radius (Figure 1c), evidence that the mROI is present in these cases. The corresponding density profiles resemble NFW profiles, *i.e.*, a scalelength is introduced. While generic equilibria do not have a unique relation between β and γ , Hansen & Moore (2004) point out that a wide variety of CNS halos appear to have a specific link between the anisotropy distribution and γ . In §5, we further discuss this connection and the specific forms of the density and anisotropy profiles.

These previous studies provide evidence of two things. One, the mROI, and its consequent anisotropy profile that has a distinct scalelength dividing an isotropic core from a radial mantle, is ubiquitous in collapses¹. Two, this scalelength is linked to (if not the same as) the scalelength of the resulting density distributions. These points are the basis of the hypothesis that the mROI a) is the key physics missing from previous AB studies of dark matter halo formation and b) leads to density profiles with scalelengths. We will now proceed to describe and discuss our testing of this hypothesis.

4. Demonstrating the Link Between Anisotropy & Density Profiles

We are not interested in modeling the mROI. What we want to do is mimic the key result of the instability, the anisotropy profile, by suitable alterations of inputs. This approach will let us test the root of the hypothesis, the impact of the anisotropy distribution on the resulting density distribution.

To create the halos we will investigate, we follow the procedure outlined in Ryden & Gunn (1987) and Williams *et al.* (2004). Initially thin spherical shells expand with the Hubble flow until they reach their turn-around radius, at which time they collapse onto the mass interior. At the moment a shell begins to collapse, the integrated effects of secondary perturbations are introduced: a shell, which can be thought of as a mass of particles, is given a velocity dispersion. This can also be pictured as giving the shell a thickness, with apo- and pericentric distances. At the same time, the perturbation velocity is oriented randomly, introducing angular momentum for that shell. The perturbation velocities calculated per Ryden & Gunn (1987) are actually RMS values. Therefore, we follow Williams *et al.* (2004) and randomly choose the magnitude of the velocity from the Maxwell speed distribution (truncated at 4 standard deviations) with the RMS value from Ryden & Gunn (1987). Since our method relies on choosing ran-

dom magnitudes and directions, for the rest of this paper we will average over some number (usually 20) of halos and refer to the average quantities as belonging to a single halo.

The benefit of the Williams *et al.* (2004) formalism is that it allows us to impose an arbitrary velocity dispersion profile and then study the halos that result from the subsequent collapse. However, before we explore variations in the anisotropy profile, we first establish a “standard” halo to use as a benchmark. By construction, it will be similar to the halos that have been created in Ryden & Gunn (1987) and Williams *et al.* (2004). The spatial density and phase-space density proxy ρ/σ^3 profiles of the standard halo are shown in Figure 2 (as usual, r_{200} is the radius at which the halo density is $200\rho_{\text{crit}}$). The top panel highlights the deviations from $\rho \propto r^{-2}$. Over a substantial radial range ($-2.5 \lesssim \log(r/r_{200}) \lesssim 0.0$), the density is well described by a single power-law $\rho \propto r^{-1.8}$. This agrees well with the halo described in Ryden & Gunn (1987, see their Figure 11). We show the ρ/σ^3 distribution for the standard halo in the bottom panel. This distribution is nicely approximated by a power-law with exponent ≈ -2 over a wide radial range $-2.5 < \log(r/r_{200}) < 0$ (Austin *et al.* 2005). We also present the velocity distributions in Figure 3. The radial, one-dimensional tangential, and total velocity dispersion profiles along with the anisotropy distribution are shown. Note that the velocities are basically isotropic over the entire range (the upturn outside r_{200} is from infalling material). Not surprisingly, given its scale-free power-law properties, we find that the standard halo is a poor match to those from cosmological N-body simulations, represented in Figure 2 by a NFW profile of concentration 10 (dash-dotted line).

We now turn our attention to altering the parameters of the standard halo by varying the velocities caused by secondary perturbations. We introduce a factor ν , which is a function of initial comoving radius x , to effect the desired changes. Since we are interested in mimicking the end result of the mROI, we introduce changes that produce an anisotropy profile that is isotropic near the center and becomes radially anisotropic with increasing radius.

The prescription for doing this in Williams *et al.* (2004) is a simple one; halve the perturba-

¹We note that this evidence cannot be considered conclusive as other studies have found that different mechanisms, most notably density inhomogeneities, can also lead to similar outcomes (*e.g.*, van Albada 1982; Londrillo, Messina, & Stiavelli 1991).

tion velocities in a specified comoving radial range $(x_{\text{lo}}, x_{\text{hi}})$ giving an inverted top-hat ν distribution,

$$\nu(x) = \begin{cases} 1 & : x < x_{\text{lo}} \\ 0.5 & : x_{\text{lo}} < x < x_{\text{hi}} \\ 1 & : x > x_{\text{hi}}. \end{cases} \quad (3)$$

In this prescription, the perturbation velocities are simply multiplied by ν . The impact of this prescription is to decrease the angular momentum imparted by perturbations in the specified radial range. This prescription also alters the total perturbation velocity, thereby changing the energy imparted to the halo by the perturbations. The end result is a halo that loses the power-law properties of the standard halo and instead resembles an NFW profile (see Figure 3 in Williams *et al.* 2004).

A representative $\nu(x)$ distribution used in this study is shown in Figure 4. The distance measure of the x -axis is the initial comoving radius of a shell in Mpc. The algebraic expression is,

$$\nu(x) = \nu^*(x) - [\nu^*(x) - d]e^{-(x-x_h)^n/2\omega^2}, \quad (4)$$

where n and ω control the shape and width of the trough, d is the depth of the trough, x_h is the mid-point of the trough,

$$\nu^*(x) = 0.5(\nu_0 - \nu_\infty)(1 - \tanh[2s(x-x_h)/(\nu_0 - \nu_\infty)]) + \nu_\infty,$$

$2s/(\nu_0 - \nu_\infty)$ controls the slope of ν^* at x_h , and ν_0 and ν_∞ are the asymptotic values. These parameters give us considerable flexibility to explore the impact of secondary perturbations on the final halos. After some experimentation, we have found that the interesting parameters to vary are ν_0 , ν_∞ , and x_h . We fix the remaining parameters; $n = 4$, $\omega = 0.4$, $d = 0.5$, $s = 20$. In general, $\nu_0 > 1$ and $\nu_\infty = 1$. If we simply multiply the perturbation velocities by ν , then near the center ($\nu > 1$) we introduce more angular momentum than in the standard halo. Conversely, $\nu < 1$ saps angular momentum relative to the standard case. Through various trials, this change from $\nu > 1$ to $\nu < 1$ appears essential to reproducing the mROI anisotropy profile, and we point out that ν is simply a means of achieving this end. We have not determined the exact link between the behavior of ν , which is imposed only at a shell's initial turn-around point, and the physical process of the mROI. It is possible that the RMS perturbations calculated according to Ryden & Gunn (1987) are larger than those

in CNS because of the one-dimensional nature of this method. If this is the case, then $\nu < 1$ is simply reducing the effects of exaggerated secondary perturbations. While further work may elucidate the relationship between ν and the physics of the mROI, for the purposes of this study, it suffices that this ν distribution gives rise to an mROI-type anisotropy profile.

As it seems unlikely that the mROI changes the energies of particles, we turn to a new prescription that leaves shell energies unchanged and instead affects the orientations of the perturbation velocities. The prescription presented here (and shown in Figure 4) uses the following ν distribution parameters; $\nu_0 = 1.6$, $\nu_\infty = 1.0$, $x_h = 0.8$ Mpc. The magnitude of the perturbation velocity remains unchanged from its value derived from the Maxwell speed distribution, but $\nu > 1$ increases the probability that the velocity is oriented tangentially and vice versa. We reiterate that this prescription is intended solely to produce an mROI-type anisotropy profile. There is no direct link between ν and the physics of the mROI, and so the correspondence between the final profiles is bound to be inexact.

Figure 5 illustrates the resulting spatial density and ρ/σ^3 profiles. We can see that adopting this new prescription has indeed provided a scale-length for the halo. While we have not set out to exactly recreate NFW halos, the similarity is clear. Some of the differences between the average and NFW profiles is due to the fact that many individual halos are good approximations to NFW profiles with different concentrations ($5 \leq c \leq 9$). Averaging these together tends to smear the peaks into a broader profile. Looking at the distribution in panel (b), we see a profile that is a decent approximation to a power-law over a couple orders of magnitude. It also appears to be a bit shallower (slope ≈ -1.8) than the standard halo's ρ/σ^3 profile and more in line with the results of Taylor & Navarro (2001) who find a slope of -1.875 for three CNS halos. Figure 6 contains the same velocity information as Figure 3. The break in the power-law that is present in the density has an analogous presence in the velocity distributions. Also, the anisotropy profile is familiar from the preceding discussion of the mROI; *i.e.*, the velocities are isotropic near the center with a fairly sharp transition to anisotropy. This result is in qualita-

tive agreement with the discussion of collapses in Merritt & Aguilar (1985); the ROI reduces the central density relative to purely radial collapses.

To this point, the discussion and figures presented in this section are all based on a single set of parameters that determine the ν distribution. We have done some parameter space exploration and have found that the ν_0 parameter can have an important impact on the final profiles. This is not very surprising, since it primarily determines the impact of the isotropic core. As ν_0 is reduced from 1.6 to 1, the inner γ of the density profile changes from ≈ 1 to ≈ 1.3 . Also, while we are not trying to exactly reproduce NFW halos, we have noted that by eliminating the introduction of random perturbation velocity magnitudes (*i.e.*, just using the RMS values) we can make the agreement between our halos (not shown) and NFW halos better. We speculate that this occurs because it provides “colder” initial conditions (in the sense discussed regarding the ROI). We also find that the anisotropy profile is hardly affected if ν_∞ is varied between 1.0 and d (the effect of changing ν_∞ is to lower the ν value from 1.0 to $d = 0.5$ over the range $1.5 \lesssim x \leq 2.5$, see Figure 4).

A more thorough investigation has been made regarding the importance of x_h , the mid-point of the ν trough. This parameter directly impacts the extent of the isotropic core present in the final anisotropy profile. In Figure 7, we show density profiles (left column) and the corresponding anisotropy profiles for 7 values of x_h surrounding the canonical value; from top to bottom $x_h = \{0.6, 0.7, 0.8, 0.9, 1.0, 1.1, 1.2\}$. We note that all the density profiles have scalelengths, but the agreement with the NFW form is within the error bars only for $x_h = \{0.7, 0.8, 0.9\}$. More importantly, these models highlight the correspondence between the density scalelength r_d and the anisotropy scalelength r_b , defined here to be the radius at which $\beta = 0.5$, as in Equation 1. Figure 8 displays this correlation (solid line) and also shows how r_i , the largest radius at which $\beta = 0$, changes with r_d (dash-dotted line). The density and anisotropy scalelengths are roughly the same (within $\approx 20\%$) in these halos, further supporting the hypothesis that mROI induced anisotropy profiles lead to scalelengths in density profiles.

5. Relating the mROI and Shapes of N-body Halo Density Profiles

In this section, we take up a discussion of the “true” shape of N-body halos. The preceding discussion has purposely ignored the differences between the “canonical” NFW profile and other CNS halo fitting functions (*e.g.*, Navarro *et al.* 2004). One must realize that our lack of detailed understanding of the physics of halo formation has forced us to approach halo structure from a very reactive posture; halos are formed and then functions are chosen that resemble the resulting density profiles. Unfortunately, these functions are somewhat arbitrary and do not, by themselves, lead to a deeper understanding of halo dynamics. The central idea of this study, that the mROI leads to an anisotropy distribution that is linked to the density distribution, can potentially provide a way around this arbitrariness. A full understanding of this physical mechanism can provide us with an expected density profile for collapse equilibria. In reality, the ROI is not fully understood and so no *ab initio* prediction can be made. At present, we are left to continue the passive role of finding the function(s) that best explain the simulation results and we now discuss the density profile specifically.

The density profile that has long been found associated with both noncosmological (*e.g.*, van Albada 1982; Londrillo, Messina, & Stiavelli 1991) and cosmological (*e.g.*, Katz 1991; Carpintero & Muzzio 1995) N-body simulations is the de Vaucouleurs (Sérsic $n = 4$) profile. However, Sérsic profiles are not very similar to the NFW profile, the dominant density fitting function over the past decade. While NFW profiles do fit CNS halo density profiles well, recent work by Navarro *et al.* (2004) suggests that the asymptotic behavior of the NFW profile as $r \rightarrow 0$ and $r \rightarrow \infty$ does not fit density profiles as well as a function similar to the Sérsic form (however, for a dissenting view see Diemand *et al.* 2005). Additionally, Dalcanton & Hogan (2001) and Merritt *et al.* (2005) have presented evidence that the Sérsic form is closer to the true shapes of halo density profiles. As the density profiles of the various ROI studies listed in this paper also find Sérsic (specifically de Vaucouleurs) profiles, the N-body findings mesh nicely with the hypothesis that the ROI is a key part of forming collapse equilibria.

Taking the link between the mROI and equilibrium density distribution as established, we now speculate about the causal relationship between them. Kazantzidis *et al.* (2004) point out that there are a wide variety of equilibria available to halos with density profiles like those from CNS. This variety arises from different velocity distributions, but we have shown that CNS halos display mROI-type anisotropy profiles exclusively (see also Hansen & Moore 2004). We propose that this choice between the equilibria is dynamically set by the mROI, which brings about the anisotropy distribution that is associated with a Sérsic density profile. As mentioned before, we cannot currently demonstrate this association analytically, but Trenti, Bertin, & van Albada (2005), following the work of Stiavelli & Bertin (1987) and Merritt, Tremaine, & Johnstone (1989), discuss how the Sérsic density profile goes hand-in-hand with the isotropic core and radially anisotropic mantle associated with the mROI. They present a distribution function meant to describe systems that have experienced incomplete violent relaxation. When this distribution function is integrated over velocity space, the density profile is very similar to the Sérsic form. Integrating this function over spatial coordinates, one derives an anisotropy profile that has the characteristic mROI shape. In the context of this idea, the link between anisotropy and density profiles is present regardless of initial conditions (*i.e.*, cosmological or noncosmological), but we speculate that such different initial conditions most likely lead to differing Sérsic n values. Returning to the “true” shape of N-body halos, we conclude that Sérsic, rather than NFW, profiles are better descriptions of the density profiles of CNS halos and that a fuller understanding of the ROI will provide insight to the actual density profiles.

6. Summary & Conclusions

There is an important difference between models of collisionless dark matter halos created from analytically-based methods and those resulting from cosmological N-body simulations. Unless the input physics (Avila-Reese, Firmani, & Hernandez 1998; Lokas 2000; Nusser 2001) or parameters are varied (as in §4), the halos that result from analytical calculations tend to be best described by a single power-law density profile and approximately

constant isotropic velocity dispersion anisotropy profiles. Cosmological N-body simulation halos tend to have density distributions that steepen and anisotropy profiles that become more radial with increasing radius.

We have explored the hypothesis, akin to the discussion in Merritt & Aguilar (1985, §6), that the presence of scalelengths in cosmological N-body simulations can be attributed to a mild aspect of the radial orbit instability, which produces equilibrium halos with isotropic cores surrounded by regions of radial anisotropy. The hypothesis is that it is this fundamental change in the character of the orbits supporting the halo that leads to scalelengths. Cosmological N-body simulation halos incorporate the physics of the mild aspect of the radial orbit instability and present such scalelengths. Analytically-based halos do not have this instability “built-in” and therefore lack the consequent scalelengths.

Utilizing an extension of the analytically-based method of Ryden & Gunn (1987), we have investigated whether or not a preferred scalelength can be introduced into a halo that would naturally have a single power-law density distribution. To mimic the impact of the mild aspect of the radial orbit instability, we have artificially altered the velocities introduced by secondary perturbations to be more tangential near the center and more radial in the outer parts of a halo. This is an approximate way to include the effect of the instability in a technique that does not explicitly include such physics. In our prescription, the magnitudes of the perturbation velocities are left unchanged, only the directions are altered. This leaves the energy budget of the halo unchanged, which we argue is an acceptable approximation to the instability. The important result is that the final halos have an anisotropy distribution reminiscent of those from cosmological N-body simulation halos and a density profile akin to an NFW profile. An exploration of the parameter space of our models shows that the presence of a scalelength is insensitive to the relative sizes of the isotropic and radially anisotropic regions, and the anisotropy radii of halos are approximately equal to their density scalelengths.

If cosmological N-body simulations are environments in which the mild aspect of the radial orbit instability plays a significant role (and they ap-

pear to be so), two central features of such simulations have a ready explanation. One is the seeming universality of halo density profiles which appears in both noncosmological and cosmological N-body simulations as Sérsic density profiles. A physical mechanism, like the mild aspect of the radial orbit instability, that generically acts in collapses, even when mergers are absent, provides a simple generator for such universality. The outcome of the instability is a variable anisotropy distribution with isotropic orbits in central regions and radially anisotropic orbits in outer regions. This anisotropy distribution gives rise to density profiles with scalelengths, the second defining feature of halos formed in cosmological N-body simulations.

We thank an anonymous referee for a careful reading and insightful comments that improved this paper. This work has been supported by NSF grant AST-0307604. Research support for AB comes from the Natural Sciences and Engineering Research Council (Canada) through the Discovery grant program. AB would also like to acknowledge support from the Leverhulme Trust (UK) in the form of the Leverhulme Visiting Professorship at the Universities of Oxford and Durham. JJD was partially supported through the Alfred P. Sloan Foundation.

REFERENCES

- Aguilar, L., Merritt, D. 1990, *ApJ*, 354, 33
- Austin, C., Williams, L. L. R., Barnes, E. I., Babul, A., Dalcanton, J. J. 2005, submitted to *ApJ*
- Avila-Reese, V., Firmani, C., Hernandez, X. 1998, *ApJ*, 505, 37
- Barnes, J., Goodman, J, Hut, P. 1986, *ApJ*, 300, 112
- Bertschinger, E. 1984, *ApJS*, 58, 39
- Binney, J., Tremaine, S. 1987, *Galactic Dynamics*, (Princeton:Princeton Univ. Press)
- Bullock, J. S., Dekel, A., Kilatt, T. S., Kravtsov, A. V., Klypin, A. A., Porciani, C., Primack, J. R. 2001, *ApJ*, 555, 240
- Carlberg, R. G., Yee, H. K. C., Ellingson, E. 1997, *ApJ*, 485, L13
- Carpintero, D. D., Muzzio, J. C. 1995, *ApJ*, 440, 5
- Cole, S., Lacey, C. 1996, *MNRAS*, 281, 716
- Dalcanton, J. J., Hogan, C. J. 2001, *ApJ*, 561, 35
- Diemand, J., Zemp, M., Moore, B., Stadel, J, Carollo, M. 2005, astro-ph/0504215
- Dubinski, J., Carlberg, R. G. 1991, *ApJ*, 369, 13
- Fillmore, J. A., Goldreich, P. 1983, *ApJ*, 281, 1
- Fridman, A. M., Polyachenko, V. L. 1984, *Physics of Gravitating Systems* (New York:Springer)
- Gott, J. R. 1975, *ApJ*, 201, 296
- Gunn, J. E., Gott, J.R. 1972, *ApJ*, 176, 1
- Gunn, J. E. 1977, *ApJ*, 218, 592
- Hansen, S. H., Moore, B. 2004, astro-ph/0411473
- Huss, A., Jain, B., Steinmetz, M. 1999, *ApJ*, 517, 64
- Jaffe, W. 1983, *MNRAS*, 202, 995
- Katz, N. 1991, *ApJ*, 368, 325
- Kazantzidis, S., Magorrian, J., Moore, B. 2004, *ApJ*, 601, 37
- Lokas, E. L., 2000, *MNRAS*, 311, 423
- Londrillo, P., Messina, A., Stiavelli, M. 1991, *MNRAS*, 250, 54
- McGlynn, T. A. 1984, *ApJ*, 281, 13
- Merritt, D. 1985, *MNRAS*, 214, 25P
- Merritt, D., Aguilar, L. 1985, *MNRAS*, 217, 787
- Merritt, D., Tremaine, S., Johnstone, D. 1989, *MNRAS*, 236, 829
- Merritt, D., Navarro, J. F., Ludlow, A., Jenkins, A. 2005, *ApJ*, 624, 85L
- Moore, B., Governato, F., Quinn, T., Stadel, J., Lake, G. 1998, *ApJ*, 499, L5

Moore, B., Quinn, T., Governato, F., Stadel, J., Lake, G. 1999, *ApJ*, 310, 1147

Navarro, J. F., Frenk, C. S., White, S. D. M. 1996, *ApJ*, 462, 563

Navarro, J. F., Frenk, C. S., White, S. D. M. 1997, *ApJ*, 490, 493

Navarro, J. F., Hayashi, E., Power, C., Jenkins, A. R., Frenk, C. S., White, S. D. M., Springel, V., Stadel, J., Quinn, T. R. 2004, *MNRAS*, 349, 1039

Nusser, A., 2001, *MNRAS*, 325, 1397

Palmer, P. L., Papaloizou, J. 1987, *MNRAS*, 224, 1043

Polyachenko, V. L. 1981, *Pis'ma Astr. Zh.*, 7, 142 (translated in *Soviet Astr. Lett.*, 7, 79)

Polyachenko, V. L., Shukhman, I. G. 1981, *Astr. Zh.*, 58, 933 (translated in *Soviet Astr.*, 25, 533)

Power, C., Navarro, J. F., Jenkins, A., Frenk, C. S., White, S. D. M., Springel, V., Stadel, J., Quinn, T. 2003, *MNRAS*, 338, 14

Ryden, B. S., Gunn, J. E. 1987, *ApJ*, 318, 15

Sérsic, J. L. 1968, *Atlas de Galaxies Australes* (Córdoba: Obs. Astron., Univ. Nac. Córdoba)

Springel, V., White, S. D. M., Hernquist, L. 2004, *IAUS*, 220, 421

Stiavelli, M., Bertin, G. 1987, *MNRAS*, 229, 61

Taylor, J. E., Navarro, J. F. 2001, *ApJ*, 563, 483

Trenti, M., Bertin, G., van Albada, T. S. 2005, *A&A*, 433, 57

van Albada, T. S. 1982, *MNRAS*, 201, 939

Williams, L. L. R., Babul, A., Dalcanton, J. J. 2004, *ApJ*, 604, 18

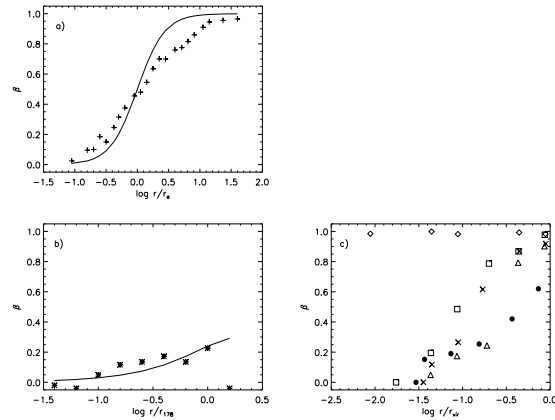


Fig. 1.— Plots showing the behavior of the anisotropy parameter β for various simulations. a) The plus symbols denote the results of van Albada (1982). The line is the initial anisotropy distribution utilized in Merritt & Aguilar (1985) (see Equation 1). b) The asterisks mark the values resulting in the $n = -2$ simulation of Cole & Lacey (1996). This line is the distribution suggested in Carlberg *et al.* (1997). c) The following symbols represent the various models described in Huss *et al.* (1999); diamonds – Model I (purely radial), triangles – Model II, squares – Model III, crosses – Model IV, filled circles – Model V.

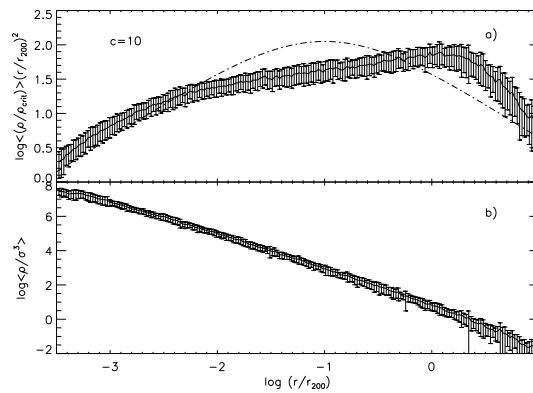


Fig. 2.— Standard halo spatial and phase-space density proxy distributions. a) Multiplying the spatial density by r^2 enhances the deviations from that power-law. The dash-dotted line is an NFW profile with a concentration of 10. b) The phase-space density proxy distribution. The $1\text{-}\sigma$ error bars are shown and the normalization is arbitrary in both panels.

This 2-column preprint was prepared with the AAS L^AT_EX macros v5.2.

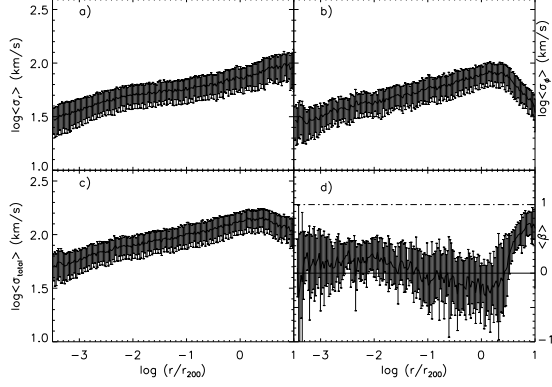


Fig. 3.— Standard halo velocity distributions. a) The radial velocity dispersion profile. b) The one-dimensional tangential velocity dispersion profile. c) The total velocity dispersion profile. d) The anisotropy profile. The dash-dotted line shows the anisotropy of purely radial orbits. The solid line is for isotropic orbits. The $1-\sigma$ error bars are shown in all panels.

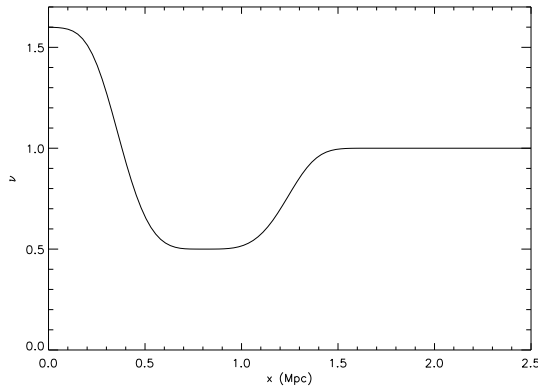


Fig. 4.— The distribution of ν values versus initial comoving radius in Mpc. See §4 for the utility of ν .

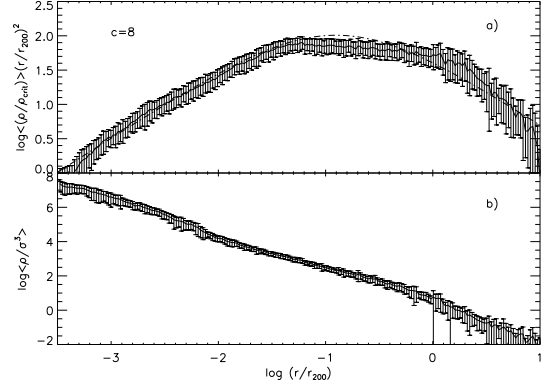


Fig. 5.— The spatial (a) and ρ/σ^3 (b) density distributions resulting from the prescription described in §4. The dash-dotted line in (a) is an NFW profile with a concentration of 8. The $1-\sigma$ error bars are shown and the normalization is arbitrary in both panels.

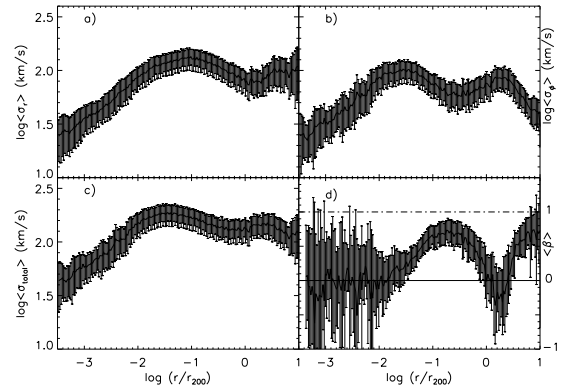


Fig. 6.— The velocity distributions resulting from the prescription described in §4. The panels are the same as in Figure 3.

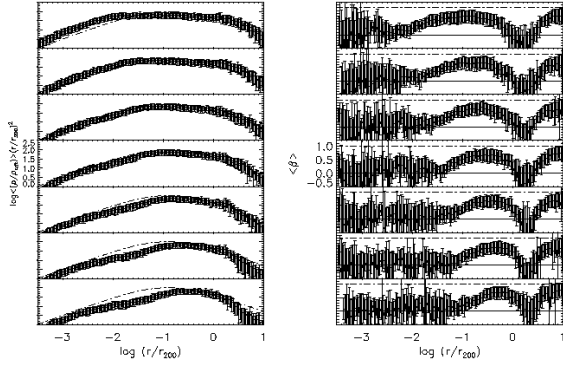


Fig. 7.— Density (left column) and anisotropy (right column) profiles for different values of x_h . From top to bottom, $x_h = \{0.6, 0.7, 0.8, 0.9, 1.0, 1.1, 1.2\}$. The dash-dotted line in the density profiles is an NFW profile with a concentration of 8. The ordinate values listed are the same for each panel in their respective columns. The solid and dash-dotted lines in the anisotropy profiles mark isotropy ($\beta = 0$) and total radial anisotropy ($\beta = 1$), respectively. Each model is the average of 10 individual halos.

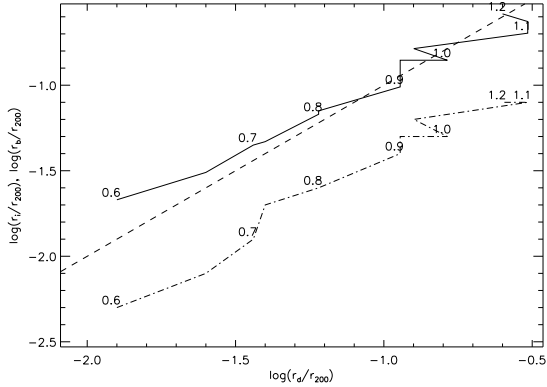


Fig. 8.— The correlations between anisotropy radius r_b (solid line) and maximum isotropic radius r_i (dash-dotted line) and the density scalelength r_d . The dashed line represents a one-to-one correspondence and the numbers are the corresponding x_h values.